Tracing of Cl input into the sub-arc mantle through the combined analysis of B, O and Cl isotopes in melt inclusions

Anne-Sophie Bouvier, Mélina Manzini, Estelle F. Rose-Koga, Alexander R.L. Nichols, Lukas Baumgartner

Tracing of Cl input into the sub-arc mantle through the combined analysis of B, O and Cl isotopes in melt inclusions.

Anne-Sophie Bouvier[1*], Mélina Manzini[1], Estelle F. Rose-Koga[2], Alexander R.L. Nichols[3], Lukas P. Baumgartner[1]

[1]Institut des Sciences de la Terre, Université de Lausanne, Switzerland

[2]Laboratoire Magmas et Volcans, Université Clermont Auvergne, France

[3]Department of Geological Sciences, University of Canterbury, New Zealand

Abstract

The effect that recycling crust and sediments have on the composition of the mantle wedge, in particular in terms of volatiles, is still debated. Chlorine, an important fluid mobile element that has stable isotopes with different concentrations in the terrestrial reservoirs, has the potential to be used to trace slab-derived fluids.

Olivine-hosted melt inclusions (OHMIs) provide a first order constraint on the $\delta^{37}Cl$ of primary magmas, since they are unaffected by near surface processes. In this study, $\delta^{37}Cl$ were coupled with $\delta^{11}B$ and $\delta^{18}O$ analyses in samples from the Lesser Antilles, Vanuatu, Aeolian, NE Japan and Izu-Bonin arcs. This unique dataset is used to better understand the large $\delta^{37}Cl$ variation in melt inclusions from a single sample. OHMIs from the Vulcano (Aeolian arc) and Sukumoyama (Izu-Bonin arc) samples have similar $\delta^{37}Cl$ (-2.5±0.5‰ and -2.6±0.8‰, respectively). These are different from $\delta^{37}Cl$ in OHMIs from the other three localities ($\delta^{37}Cl$ of -0.7±0.6‰ for Aoba (Vanuatu arc) and St. Vincent (Lesser Antilles arc), -

1±0.9‰ for Iwate (NE Japan)). Vulcano OHMIs also have statistically different B and O isotope compositions compared to those from the other locations: average $\delta^{11}B$ of -5.1±2.9‰ for Vulcano OHMIs, compared to 2.5±3.7‰, 5.2±1.4‰, 7.0±2.2‰, 3.8±7.5‰ for Sukumoyama, Iwate, Aoba and St. Vincent OHMIs, respectively. All OHMIs have $\delta^{18}O$ between 4.0 and 7.4‰, except for those from Vulcano, which are significantly different, with $\delta^{18}O$ from 7.2 to 9.1‰. Combining these three stable isotope systems suggests that the large variation (>2‰) of $\delta^{37}Cl$ in OHMIs from a sample reflects inputs from different sources of Cl rather than heterogeneities in a single main source. Variability between arcs might reflect different major sources of Cl.

Comparing OHMIs Cl isotope data from the Aeolian and Izu-Bonin arcs with existing bulk rock Cl isotope data suggest that OHMIs preserve the source signature of Cl input whereas this signal can be lost in whole rocks as a result of Cl isotope diffusive fractionation during Cl degassing. SIMS measurements of Cl isotopes in OHMIs could thus help refine models of Cl cycles in the mantle.

Keywords: melt inclusions; chlorine isotopes; oxygen isotopes; boron isotopes; subduction zones; SIMS

1. Introduction

Chlorine has been widely studied as an element in volcanic systems (e.g., Aiuppa et al., 2009; Mather et al., 2012), but to date only a few studies have reported Cl isotopes (noted $\delta^{37}Cl$) in rocks and minerals and used them to make petrogenetic interpretations (~35 papers since 1995 and a few pioneering works prior to that). After some debate about the Cl isotope values of the terrestrial reservoirs, refinement of bulk rock analytical techniques has brought

scientists to a consensus on the relatively narrow range of $\delta^{37}Cl$ found in terrestrial rocks (Figure 1 and Supplementary material 1). In subduction zones, Cl, a soluble element, could serve as a tracer of different Cl sources that contaminate the mantle wedge. Based on theoretical calculations (Schauble et al., 2003) and experimental work (Liebscher et al., 2006), fractionation of Cl isotopes between silicates and NaCl at T >300°C should be limited. This implies that $\delta^{37}Cl$ should not be (or only slightly) fractionated during slab dehydration (Barnes et al., 2006; Bonifacie et al., 2008; John et al., 2011). The isotopic composition of a metasomatized mantle should thus reflect simple binary mixing between the host rock and the metasomatizing agent. The $\delta^{37}Cl$ of arcs lavas vary from -2.6 to +3.0‰ (e.g., Barnes et al., 2009; Barnes and Straub, 2010). These studies have been used to estimate the Cl reservoirs and suggested that Cl could be derived from altered oceanic crust (AOC), serpentinites or sediments, depending on the depth of fluid extraction, which leads to a change in $\delta^{37}Cl$ across an arc (Barnes et al., 2008). Variation along the Central America volcanic arc has also been observed and has been used to suggest different sources of Cl along the arc (Barnes et al., 2009).

Recently, Manzini et al. (2017) reported $\delta^{37}Cl$ in olivine-hosted melt inclusions (OHMIs) from three different arc settings (the Lesser Antilles, Aeolian and Vanuatu arcs). Their study reported large intra-sample $\delta^{37}Cl$ variations (up to 2.5‰, Figure 1) that are half of the variation exhibited by all the bulk rocks from arc settings measured to date. Two arcs display similar $\delta^{37}Cl$ (-1.9 to +0.6‰), whereas the third one has significantly different $\delta^{37}Cl$ compositions (-3.4 to -2.0‰). These authors suggested that for the Lesser Antilles and Vanuatu arcs, $\delta^{37}Cl$ in the OHMIs reflect the imprint of serpentinite (and/or AOC) whereas for the Aeolian arc, $\delta^{37}Cl$ is influenced by sediments. The difference between the two different sets of compositions might reflect the different slab geometries that the arcs have.

As pointed out by Manzini et al. (2017), further work was required to better understand the different $\delta^{37}Cl$ compositions between the three different arcs, as well as the relatively large variation observed within a sample. Also, new data published for bulk rocks in the Aeolian arc show large $\delta^{37}Cl$ difference between Stromboli lavas (-0.96 to +0.69‰; Liotta et al., 2017) and Stromboli OHMIs (-3.2 to -1.75‰; Manzini et al., 2017). In order to understand the large variations and assess how representative the $\delta^{37}Cl$ values recorded in OHMIs are, this study couples $\delta^{37}Cl$ data obtained by Manzini et al. (2017) with $\delta^{11}B$ and $\delta^{18}O$ obtained in the same OHMIs. In addition, new Cl, B and O data from two additional arcs (Izu-Bonin and NE Japan) have been acquired. Oxygen isotopes do not largely fractionate during dehydration at high temperature (e.g., Liebscher et al., 2006; Schauble et al., 2003; Zheng, 1993). Comparison of these two isotopic systems allows sediment vs. AOC/serpentinite influences to be identified. In contrast to O and Cl isotopes, B isotopes largely fractionate during dehydration (e.g., Ishikawa & Nakamura, 1994; Peacok & Hervig, 1999), complicating the data interpretation due to the lack of B isotope partitioning data in the different phases involved. However, B isotopes have the potential to distinguish between AOC and serpentinites end-members as their respective bulk rocks are different (Boschi et al., 2013; Chaussidon & Jambon, 1994; Smith et al., 1995; Vils et al., 2009). This unique dataset combining Cl isotopes with two other stable isotope systems in melt inclusions is used to assess if variations of $\delta^{37}Cl$ in melt inclusions within a sample represent heterogeneities in a single, major, Cl reservoir, or alternatively reflect that Cl is added to the mantle wedge from different sources. Disparities between the whole rocks and OHMIs are also discussed in terms of analytical artefacts and/or fractionation due to diffusion.

2. Geological context and sample descriptions

All samples were previously studied and their geological settings are well-known. They were chosen as they contain glassy OHMIs with basaltic compositions, potentially providing access to Cl-undegassed melts. The different arcs have been chosen to represent various amounts of fluids involved in their magma genesis (see section 2.1). They are thus suitable samples to test whether $\delta^{37}Cl$, coupled with other isotopic systems, could be a useful tracer of Cl sources and the fate of Cl in subduction zones.

2.1. Melt inclusions from previous studies

OHMIs from St. Vincent (Lesser Antilles arc), Vulcano (Aeolian arc) and Aoba (Vanuatu arc) are the same as those reported by Manzini et al. (2017). OHMIs from Iwate Volcano (NE Japan arc) were analyzed for volatiles by Rose-Koga et al. (2014). Nomenclature of each OHMI is identical to their original papers.

The intra-oceanic volcanic arc of the Lesser Antilles arc is generated by the subduction of the Atlantic Plate beneath the Caribbean Plate (see Macdonald et al., 2000 for a review). Analyzed OHMIs were separated from a lapilli deposit collected near Troumaka Bay, in St. Vincent, where high-MgO basalts occur. Based on B isotopes, Bouvier et al. (2008) suggested that fluids involved in the magma genesis are derived from serpentinites, sediments and AOC. The Aeolian arc is related to the subduction of the Ionian-Adriatic lithosphere underneath the Calabrian arc. Mantle beneath the Aeolian arc volcanoes has been metasomatised by fluids from the Ionian oceanic crust and the sediments from the Ionian basin in the eastern part of the arc (Peccerillo et al., 2013). The selected OHMIs come from La Sommata scoria cone on Vulcano Island. OHMIs from Stromboli, analyzed for $\delta^{37}Cl$ by Manzini et al. (2017), were not included in this study as they were too small to undergo further analysis.

The Vanuatu arc is generated by the northeastward subduction of the Australian Plate beneath the Pacific Plate. The selected olivine crystals come from three different lapilli layers

of Aoba Island (Ao3 from an eruptive fissure on the volcano north flank; Ao15 from Torgil tuff ring; and Ao17 from Red Cliff pyroclastic sequence; Sorbadere et al., 2011). Slab fluids beneath Aoba involved fluids derived from serpentinites (Métrich and Deloule, 2014).

NE Japan arc is generated by the subduction of the Pacific Plate beneath the Okhotsk Plate. The sample, coming from arc front Iwate Volcano, was studied by Rose-Koga et al. (2014). These authors showed that fluids from the slab beneath Iwate Volcano are derived from AOC and sediments. The selected OHMIs have already been analyzed for major and volatiles elements, and Pb isotopes, and have been chosen based on their size – they have to be large enough to place a δ^{37}Cl SIMS spots in between previous SIMS spots.

2.2. New melt inclusions from Izu-Bonin arc

New data for OHMIs from a sample collected from the Sukumoyama scoria cone in the Higashi-Izu Monogenetic Volcano Field (HIMVF), on the northeastern Izu Peninsula, were used in this study. The Izu-Bonin arc is an intraoceanic arc generated by the subduction of the Pacific Plate beneath the Philippine Sea Plate. Since 15 Ma, the Izu-Bonin arc has been colliding with the Honshu Arc in central Japan to form the Izu collision zone. OHMIs from sample IZ27-15 on Sukumoyama were analyzed previously for major, volatile and trace elements (Nichols et al., 2012). Compositional variations were suggested to reflect interstitial melts within the crystal mush of the magma chamber experiencing distinct crystallization histories and variability between contributions from fluid and sediment melt components in the source. For this study, new OHMIs were polished and analyzed from the same sample used by Nichols et al. (2012).

3. Methods

143 Olivine crystals from the 0.5-1 mm grain size fraction of crushed scoria were hand-picked
144 under a binocular microscope and embedded in epoxy. Olivine crystals containing naturally
145 glassy OHMIs were polished individually in order to expose the OHMI on the surface. Most
146 OHMIs contain a shrinkage bubble, but none contain daughter minerals. Each polished
147 olivine was removed from epoxy and pressed into indium, along with various reference
148 materials for secondary ion mass spectrometry (see below). Each analytical method applies
149 for all OHMIs.

150 *3.1.Electron microprobe (EMPA)*

151 Major element compositions of the MIs and their host olivine were acquired by electron
152 microprobe (EMPA) using a JEOL 8200 Superprobe. For the MIs, analytical conditions were
153 15kV, 10nA current and a 5 μm beam while conditions were 15kV, 15 nA, 1 μm, for the
154 olivine host. Peak counting times were 30 s on all elements, except for K, Na and Ca (20 s).
155 Backgrounds were counted for 15 or 10 s (Si, Fe, Na, Ca, K). Cl was determined by EMPA
156 only in OHMIs analyzed by Manzini et al. (2017); for other OHMIs, Cl content was measured
157 using SIMS. For the MIs, the KL2-G glass standard (Jochum et al., 2006) was used to
158 calibrate SiO_2 and Al_2O_3. Other elements were calibrated on different minerals. ML3B-G
159 (Jochum et al., 2006) and San Carlos olivine were used as internal standards to check the
160 calibration.

161 *3.2.Secondary Ion Mass Spectrometry (SIMS)*

162 Boron, Cl and O isotope ratios were measured by secondary ion mass spectrometry
163 (SIMS) using the CAMECA IMS 1280-HR at the SwissSIMS laboratory (University of
164 Lausanne, Switzerland). A 1.5-2 nA, 10 kV Cs^+ primary beam was used to analyze Cl and O
165 isotope ratios, over two different sessions. The electron flood gun, with normal incidence, was
166 used to compensate charges. For $\delta^{37}Cl$, the analytical method was the same as described in

Manzini et al. (2017). To summarize, a pre-sputtering of 240 s with a 25 μm raster size was used in order to remove all the possible Cl contamination. Analysis time was 240 s with a 10 μm raster. $^{35}Cl^-$ and $^{37}Cl^-$ were measured simultaneously on two Faraday cups (FCs), using 10^{11} Ω resistors, with a mass resolving power (MRP) set to ~3000. The internal uncertainty (single measurement) for the samples was 0.15-0.5‰ (two standard errors, 2 s.e.), depending on the Cl content. Reproducibility (point to point) was checked using an in-house Cl-enriched standard UNIL_Gl-B7. Reproducibility of UNIL_Gl-B7 over eight points at the beginning of each session was <0.2‰ (two standard deviations, noted 2 SD hereafter), but up to 0.35‰ 2SD over a session (24-36h; two measurements of UNIL_Gl-B7 every six unknowns). Instrumental mass fractionation (IMF), depending on Si, K, and Al mole content of the glasses was calibrated using six glass standards (Manzini et al., 2017), including UNIL-Gl-B7 at the beginning of each session (SM 2A). To that purpose, UNIL_Gl-B4, UNIL_Gl-B6, RMR, PR2 and IB94 were measured four times at the beginning of each session, with two measurements of UNIL_Gl-B7 in between each different glasses. To ensure the validity of the calibration over the session and determine the uncertainty of the calibration, UNIL_Gl-B6 and UNIL_Gl-B4 were measured repeatedly over the session. A reproducibility of 0.3‰ and a maximum uncertainty of 0.4‰ were calculated. The IMF applied to each OHMIs was calculated based on their major element composition, measured by EMPA before the SIMS sessions. $\delta^{37}Cl$ is referenced to the standard mean ocean chloride (SMOC) $^{37}Cl/^{35}Cl$ ratio of 0.319592.

The Cl content of each OHMI could be estimated based on the ^{35}Cl count per second normalized to the primary beam intensity and compared to the standards. As the estimation by SIMS gives satisfactory results for Cl content <3000 ppm (SM 2B), SIMS was used to estimate the Cl contents of the new Sukumoyama OHMIs, which should have relatively low Cl contents based on those previously analyzed (Nichols et al., 2012).

192 ^{16}O and ^{18}O secondary ions were analyzed at 2400 MRP and collected on two FCs in
193 multi-collection mode using 10^{10} and 10^{11} Ω resistors, respectively. The FCs were calibrated
194 at the beginning of the session, using the calibration routine. Mass calibration was performed
195 at the beginning of each session (<12h). Each analysis takes ~4 minutes, including pre-
196 sputtering (30 s) and automated centering of secondary electrons. Ion mass fractionation was
197 calibrated using several standards with different major element compositions (SM 2C).
198 Reproducibility of the standards is better than 0.3‰. $\delta^{18}O$ is referenced to the standard mean
199 ocean water (SMOW) $^{18}O/^{16}O$ ratio of 2005.2×10^{-6}.

200 To determine $\delta^{11}B$, ^{10}B and ^{11}B were measured in multicollection mode, using two electron
201 multipliers. The O^- primary beam intensity was 8 nA and mass resolution was set at 2400. A
202 single analysis (60 cycles) took 16 minutes. The instrumental isotopic fractionation was
203 determined by analyzing five standards with different major element compositions (SM 2D).
204 As already reported in the literature, instrumental isotopic fractionation was observed to be
205 independent of major element composition (Rosner et al., 2008). Reproducibility on the
206 standards varies from 2 to 4‰ (2SD), depending on the B content of individual melt
207 inclusions. $\delta^{11}B$ is referenced to the NBS 951 $^{11}B/^{10}B$ ratio of 4.044.

208 Amongst the standards used for $\delta^{11}B$ and $\delta^{18}O$ calibrations, BHVO-2G and BCR-2G, with
209 compositions encompassing those of our OHMIs, were also included in the sample mounts, as
210 well as in the standard mount. During the session measuring $\delta^{18}O$ and $\delta^{11}B$, several analyses
211 of BHVO-2G and BCR-2G were undertaken before and after a maximum of 18 unknowns to
212 monitor instrument stability (i.e., magnetic field stability). These standards were also treated
213 as unknowns to check the accuracy of the calibration. Accuracies were similar to
214 reproducibility: 0.3‰ for $\delta^{18}O$ and 3‰ for $\delta^{11}B$.

215

4. Results

4.1.Elemental geochemistry of melt inclusions

All major elements, as well as details of the post-entrapment crystallization (PEC) corrections are reported in SMs 3-4. Compared to whole rocks from each locality, OHMIs plot at the primitive end of the differentiation trends (SM 5), and have basanite to basaltic compositions (Figure 2). The OHMIs from the different settings define distinct trends that show variable alkali enrichment, with some of St. Vincent OHMIs being the most alkali-rich, and those from Iwate Volcano, NE Japan arc, the most alkali-poor.

Manzini et al. (2017) showed that the highest and most variable Cl contents are in OHMIs from Aoba (0.06 to 0.39 wt%) and Vulcano (0.14 to 0.44wt%) islands, whereas in St. Vincent samples the range is more restricted (0.08 to 0.15 wt%). Rose-Koga et al. (2014) reported 0.03 to 0.05 wt% for Iwate OHMIs. The new data for OHMIs from Sukumoyama provide Cl contents from 0.04 to 0.09 wt%, similar to the values published by Nichols et al. (2012).

4.2.Stable isotope compositions

4.2.1. Chlorine isotopes

All stable isotope compositions are reported in Table 1. The six new data from Iwate Volcano range from -2.1±0.8‰ (2 s.e.) to 0.5±0.8‰ (2 s.e.) (average of -1‰), similar to St. Vincent and Aoba OHMIs. The nine data from Sukumoyama OHMIs show distinct values compare to Iwate Volcano OHMIs, ranging from -4.4±0.5‰ (2 s.e.) to -1.6±0.4‰ (2 s.e.) (average of -2.3‰), more similar to Vulcano. As for Vulcano OHMIs, Cl isotopes for Sukumoyama OHMIs can be compared to δ^{37}Cl bulk rock values. Indeed, lavas from two volcanoes, Oshima and Niijima, located relatively close to Sukumoyama, at the northern end of Izu-Bonin arc have been measured for δ^{37}Cl (Barnes et al., 2008). Oshima and Niijima

239 lavas have significantly higher Cl isotope compositions (-0.28‰ and -0.77‰, respectively)
240 compared to Sukumoyama OHMIs.

241 The lowest δ^{37}Cl value measured for a Sukumoyama OHMI, -4.4±0.5‰ (2 s.e.), is the
242 lowest measured for any OHMI to date and also lower than bulk rock values for solid
243 geological samples (Figure 1). This value has been carefully checked to assess its validity: all
244 SIMS analytical conditions are similar to other MIs measurements (secondary deflectors,
245 primary intensity, topography, etc). Despite the fact that this inclusion also has the lowest Cl
246 content of Sukumoyama MIs (400 ppm), analytical artefact due to low Cl content is
247 discarded: internal error (counting statistic of a single measurement; 0.5‰, 2 s.e.) is similar to
248 the internal error of other OHMIs from this sample. Additionally, some Iwate OHMIs have as
249 low as, or even lower, Cl contents (300-400 ppm) and yet δ^{37}Cl for these inclusions is in the
250 range of published values (-1.6 to +0.5‰). Hence the value is considered to be reliable.

251 4.2.2. Boron isotopes

252 The lowest δ^{11}B values have been measured in the St. Vincent OHMIs, with values
253 ranging from -18.5±1.9 to +11.7±1.9‰ (2 s.e.) (average: +3.6‰). This range, similar to the
254 range previously reported for St. Vincent OHMIs (-25.6 to +11.8‰, average 0.9‰; Bouvier
255 et al., 2008) is by far the largest range of δ^{11}B values reported for a group of OHMIs in this
256 study. δ^{11}B range from -9.5±1.9 to -1.0±2.1‰ (2 s.e.) (average: -5‰) for the Vulcano
257 OHMIs. Aoba OHMIs have positive δ^{11}B values (+3.4 to +12.0, average of +7‰), higher than
258 the values reported for MIs from two other Aoba samples (-11.9 to +6.4‰; Métrich and
259 Deloule, 2014). Sukumoyama OHMIs have variable δ^{11}B values, ranging from -4.8±4‰ to
260 +5.8±4‰ (2 s.e.) (average: 1.7‰). Iwate Volcano OHMIs have a restricted range of positive
261 δ^{11}B values (+4.7± 1.7‰ to +8.1±2‰; average: 6.3‰).

262 4.2.3. Oxygen isotopes

263 The $\delta^{18}O$ varies from 4.3±0.4 to 6.9±0.4‰ (2 s.e.), with an average of 5.8‰ for the St.
264 Vincent OHMIs, similar to the average (6.0‰) $\delta^{18}O$ reported by Bouvier et al. (2008). Aoba
265 OHMIs have a similar range of $\delta^{18}O$ composition, from 4.4±0.2 to 7.0±0.2‰ (2 s.e.)
266 (average: 6.3‰); and Sukumoyama OHMIs also have a similar range of $\delta^{18}O$ (4.8±0.3 to
267 7.4±0.3‰, 2 s.e.), but with slightly higher average (6.6‰). In contrast, Iwate Volcano OHMIs
268 have slightly lower $\delta^{18}O$ values of 3.9±0.3 to 6.6±0.3‰ (2 s.e.), with an average of 5.4‰.
269 Vulcano OHMIs have the highest $\delta^{18}O$ measured in this study. They vary from 6.1±0.2 to
270 9.1±0.2‰ (2 s.e.), with an average value of 7.9‰.

271

272 **5. Discussion**

273 *5.1. Significance of $\delta^{37}Cl$ variation in OHMIs within a sample*

274 Manzini et al. (2017) reported the first data of $\delta^{37}Cl$ in OHMIs from arc settings and
275 showed that Cl isotopes can vary by up to 2.5‰ within a single sample (St. Vincent). Here,
276 the OHMIs from two new samples from Iwate Volcano and Sukumoyama have variations in
277 $\delta^{37}Cl$ of 2.6 and 2.8‰, respectively, further confirming that relatively large variations (>2‰)
278 in Cl isotopes within OHMIs from a single sample might be common. Given the large range
279 of $\delta^{37}Cl$ in terrestrial Cl reservoirs (Figure 1), the measured variation in OHMIs within a
280 sample could reflect either heterogeneity of a single Cl reservoir, or contributions from
281 different Cl reservoirs. To better understand the variability of $\delta^{37}Cl$ within a sample, O and B
282 isotopes were measured in the same OHMIs. As mentioned in the introduction, comparison
283 with O isotopes could help to distinguish between the influence of fluids from sediments and
284 the influence of fluids from AOC/serpentinites, whereas B isotopes may differentiate between
285 fluids from AOC and serpentinites.

286 5.1.1. Are the measured $\delta^{37}Cl$ representative of the source?

287 Before any interpretation of source process(es), it is important to evaluate several potential
288 processes that can disturb the measured $\delta^{37}Cl$. First, we ensured that the selected OHMIs have
289 not degassed Cl. In a plot of SiO_2 vs. Cl content of the OHMIs (Figure 3), within each sample
290 Cl remains constant over the SiO_2 variation. This suggests that Cl is not degassing from the
291 melts as they were trapped.

292 Analytical artefacts were also investigated. Uncertainty in the calibration for Cl isotopes is
293 0.4‰ (2SD), smaller than the observed variation within a sample (> 2‰) or between samples.
294 The absence of correlation between $\delta^{37}Cl$ and SiO_2 (Figure 4A) and $Na_2O + K_2O$ (Figure 4B)
295 illustrate that the different $\delta^{37}Cl$ measured in Vulcano and Sukumoyama OHMIs compared to
296 other OHMIs (Fig. 1) is not an analytical artefact. Indeed, OHMIs from these two samples
297 have different Cl contents (>3000 ppm and <1000 ppm, respectively) and major element
298 compositions (Figure 2, SMs 3 to 5). Since calibrations were made with the same standards
299 for all samples, and that OHMIs are corrected for IMF using their own major element
300 compositions, it cannot be argued that the low $\delta^{37}Cl$ values in the OHMIs are induced by
301 analytical bias. The absence of correlation between $\delta^{37}Cl$ and SiO_2 and $Na_2O + K_2O$ within a
302 sample (Figure 4) also suggests no fractionation of $\delta^{37}Cl$ during magmatic evolution or due to
303 variable degrees of melting.

304 We have also evaluated the effects of secondary processes (e.g, PEC, shrinkage bubble).
305 Given that Cl is an ultra-trace element (<1ppm) in magmatic olivine (e.g., Urann et al., 2017),
306 late crystallization of olivine on the wall of OHMIs should not strongly affect the Cl
307 composition and Cl isotopes of OHMIs. This is verified by the absence of any relationship
308 between $\delta^{37}Cl$ and the extent of PEC. Shrinkage bubbles can contain volatile elements, mostly
309 CO_2 (e.g., Moore et al., 2015). So far, Cl content in such bubbles have not been determined.
310 Most of the OHMIs analyzed here have a shrinkage bubble inside. Several olivines contain

two or three OHMIS, but only one olivine contains two OHMIs with one containing a bubble and the other not (Aoba 3-1a and b). The one without bubbles contain 300 ppm less Cl than the one with a bubble, but the two OHMIs have similar δ^{37}Cl, within error (-0.5±0.2 and -0.7±0.2‰; SMs 3-4). Also, within a sample, the range of Cl content and δ^{37}Cl are similar for OHMIs with or without a shrinkage bubble. We thus conclude that the presence of a shrinkage bubble does not affect Cl isotopes of OHMIs. This is further confirmed by the absence of a correlation between δ^{37}Cl and Cl/K_2O (Figure 5), suggesting no Cl degassing syn- or post-entrapment. Also, Cl is not affected by diffusive re-equilibration through the host olivine (Bucholz et al., 2013). All this information suggests that the measured δ^{37}Cl are representative of the melt in which the olivine grew.

5.1.2. Cl and O isotope systematics

In a plot of Cl isotopes compared to O isotopes, AOC and serpentinite fields are distinct from the field for sediments (Figure 6 and references in the caption). Oxygen isotope fractionation between hydrous minerals and fluids at high temperature is relatively small (for example, at 500°C, ~-1.5‰ for serpentinite, amphibole; Zheng, 1993). Also, Cl isotopes in metamorphosed serpentinites and AOC are similar to those in fresh corresponding lithologies, suggesting that δ^{37}Cl do not fractionate in fluids during the dehydration of mafic lithologies (Barnes et al., 2006; Bonifacie et al., 2008; John et al., 2011). Thus, the Cl-O isotope systematics in the OHMIs from each location have been compared to these end-members (Figure 6). In all the data taken together, Cl isotopes are negatively correlated with O isotopes, with the lowest δ^{37}Cl observed in OHMIs with highest δ^{18}O and vice versa. In detail, the OHMIs from St. Vincent and Iwate Volcano display a negative relationship, whereas no systematic could be described for those from Vulcano, Aoba and Sukumoyama. There is

greater variation in $\delta^{18}O$ data at low $\delta^{37}Cl$ (< -1.6‰). The lowest bulk $\delta^{37}Cl$ (down to -3‰) and the highest bulk $\delta^{18}O$ (> 9‰) have been observed in fresh sedimentary rocks, suggesting that the low $\delta^{37}Cl$ (<-2‰) associated with high $\delta^{18}O$ (>7‰) in the OHMIs do probably reflect the influence of fluids derived from sediments. The increased scatter of the OHMIs toward this end-member could be explained by the large range of subducted sediment compositions (carbonates, silicic sediments, shales, e.g., Bindeman, 2008 for a review).

High $\delta^{37}Cl$ (>0.5‰) associated with low $\delta^{18}O$ (<5.5‰) point toward an AOC or serpentinite end-member. In detail, the coupled $\delta^{37}Cl$ and $\delta^{18}O$ values reported for fresh serpentinite rocks formed at more than 100°C suggest that $\delta^{18}O$ increases with $\delta^{37}Cl$ in serpentinites (Bonifacie et al., 2008; Boschi et al., 2013). A fluid derived from fresh oceanic serpentinites would have a $\delta^{18}O$ value 1.8‰ higher than the bulk rock it is derived from (Zheng, 1993) considering serpentinite dehydration at ~680°C (antigorite breakdown, e.g., Trommsdorff et al., 1998). Thus, a fluid escaping a serpentinite with $\delta^{37}Cl$ of ~1‰ and $\delta^{18}O$ from 4.5 to 7‰, based on the literature, will have a $\delta^{18}O$ composition >6.3‰. Such $\delta^{18}O$ is too high to explain the highest $\delta^{37}Cl$ end-member influencing the compositions of three out of four of the OHMIs with $\delta^{37}Cl$ > 0‰. Subducted serpentinites with higher $\delta^{37}Cl$ have been reported (up to 2.4‰, Barnes et al., 2006, 2013, 2014). In subducted serpentinite samples for which $\delta^{37}Cl$ and $\delta^{18}O$ have been determined, the same tendency of $\delta^{37}Cl$ to increase with $\delta^{18}O$ is observed (Barnes et al., 2014), leading to a similar conclusion as for the fresh oceanic serpentinites: a fluid escaping high $\delta^{37}Cl$ subducted serpentinites might have a $\delta^{18}O$ too high to explain the composition of OHMIs with $\delta^{37}Cl$ > 0‰. AOC, especially high temperature altered portions, have high $\delta^{37}Cl$ (up to +1.6‰; Barnes and Cisneros, 2012) and could have low $\delta^{18}O$ (down to 3‰ for the bulk rock (Alt & Bach, 2006); even as low as 0‰ for amphibole veins (Muehlenbachs, 1986)). If we assume a temperature of dehydration for

amphibole of ~500°C (blueschist – eclogite transition), a dehydration fluid from amphibole veins would have $\delta^{18}O$ ~1.7‰ higher than the dehydrating lithology/mineral (Zheng, 1993). Thus, local dehydration fluids from lower AOC could have $\delta^{18}O$ values as low as 1.7‰, making amphibole-bearing AOC a more suitable candidate for the high $\delta^{37}Cl$ - low $\delta^{18}O$ end-member of the correlation. However, in detail, the Aoba OHMIs do not follow the general trend and might also point toward a serpentinite fluid end-member.

Following this reasoning, Vulcano and Sukumoyama OHMIs, with lower $\delta^{37}Cl$ and higher $\delta^{18}O$ than MORB (Sharp et al., 2007), possibly record the strongest influence from sediment derived fluids. St. Vincent and Iwate Volcano OHMIs, which have $\delta^{37}Cl$ and $\delta^{18}O$ both higher and lower compared to DMM, suggest that melts were influenced by a fluid possibly derived from the lower AOC and also some sediments. Aoba OHMIs also have both higher and lower $\delta^{37}Cl$ and $\delta^{18}O$ compared to DMM, suggesting influence from sediment fluids and AOC or serpentinite fluids.

It is important to note that contrary to the possible AOC and/or serpentinite end-member, which does not seem to have suffered fractionation of Cl isotopes during dehydration, as previously suggested (Barnes et al., 2006; Bonifacie et al., 2008; John et al., 2011; Schauble et al., 2003), the sediment end-member probably has fractionated at some point, as some OHMIs have $\delta^{37}Cl$ values lower than the lowest $\delta^{37}Cl$ reported for bulk sediments. This observation agrees with John et al. (2010), who suggest preferential loss of ^{35}Cl from sediments into pore fluids, even at high temperature, leads to enrichments in $\delta^{37}Cl$ in recycled subducted marine sediments.

5.1.3. Cl and B isotope systematics

The distinction between AOC and serpentinite derived fluids is not unique due to their similar $\delta^{18}O$ and $\delta^{37}Cl$. Here, we investigate whether they can be distinguished in terms of

383 their Cl-B isotope systematics (Figure 7). To date, Cl isotopes have not been coupled with B
384 isotopes in the same rock samples. Fields for the different lithologies were thus assembled
385 from different samples and different settings. Cl isotope values are given in SM 1. For B
386 isotopes, sediment values are from Smith et al. (1997) and Ishikawa and Nakamura (1993);
387 The AOC values are from Smith et al. (1995), and serpentinite values are from Boschi et al.
388 (2013) and Vils et al. (2009). For reference, the MORB field is also plotted using the data for
389 $\delta^{11}B$ from Chaussidon and Jambon (1994) and for $\delta^{37}Cl$ from Sharp et al. (2007).

390 Boron isotopes fractionate strongly during dehydration, with ^{11}B partitioning
391 preferentially into the fluid phase (e.g., Peacok & Hervig, 1999; Ishikawa & Nakamura,
392 1994). Thus, B isotopes of the rock reservoirs cannot be directly compared to MI data. A
393 simple open system Rayleigh distillation is used to estimate the theoretical composition of the
394 dehydration fluids (Bouvier et al., 2010; Rose et al., 2001). For these calculations, B isotope
395 fluid-rock partition coefficients of 3-5 ‰ for serpentinites (Tenthorey and Hermann, 2004);
396 and 5‰ for AOC and sediments (You et al., 1996) were used.

397 There is no simple relationship between Cl and B isotopes for the OHMIs (Figure 7).
398 Instead, for the whole dataset, different end-members are needed to explain the variations of
399 $\delta^{11}B$ and $\delta^{37}Cl$ in OHMIs. A first fluid end-member with $\delta^{11}B$ >12‰ and $\delta^{37}Cl$ between -2
400 and -0.5‰ could be described, most probably representing the influence of fluids derived
401 from serpentinite dehydration. Indeed, amongst the three major Cl reservoirs shown in Figure
402 7, serpentinite rocks form the reservoir with the highest $\delta^{11}B$. Based on the Rayleigh
403 distillation calculation, a fluid derived from the dehydration of serpentinites with an initial
404 average $\delta^{11}B$ composition of 20‰ (Figure 5) would have $\delta^{11}B$ down to ~15‰ after 75% of B
405 loss from serpentinite.

406 A second end-member can be described by higher $\delta^{37}Cl$ (>1‰) and lower $\delta^{11}B$ (<~4‰).
407 High $\delta^{37}Cl$ have been reported for AOC with a lithology containing amphiboles (Barnes and

Cisneros, 2012) or for metamorphosed serpentinites (Barnes et al., 2014). Based on Figure 6, OHMIs with $\delta^{37}Cl > 0‰$ most likely record the influence of fluids released from amphibole bearing- lower AOC. If an influence from an AOC dehydration fluid is assumed, with initial AOC average B isotopes composition of 3‰, $\delta^{11}B$ of ~4‰ would suggest that a fluid escaping from an AOC lithology would have lost ~50% of B.

Finally, the last end-members most probably represent fluids from the subducted sediments, as suggested by Figure 6. Indeed, the lowest $\delta^{37}Cl$ are measured in sedimentary rocks (Figure 1). Likewise, extremely low $\delta^{11}B$ (<-15‰) measured in OHMIs are generally associated with the influence of fluids lost by dehydrated sediments - be they melts or fluids - derived from such a lithology (e.g., Bouvier et al., 2010; Rose et al., 2001). Interestingly, Sukumoyama and Vulcano OHMIs seem to require two distinct sediment end-members, as in Figure 6 (thus OHMIs with similar $\delta^{37}Cl$, but different $\delta^{18}O$ and $\delta^{11}B$). This distinction could reflect different degrees of dehydration of the sediment lithology. However, due to the relatively small fractionation factor for O isotopes in the fluid at high temperature (650°C, -0.4 and 1.8‰ for quartz and calcite; Zheng et al., 1993, 1999), different degrees of dehydration of similar sediment lithologies would not explain the different $\delta^{18}O$ of Vulcano and Sukumoyama OHMIs. When compared to sediment bulk rock data, continental sediments have lower $\delta^{11}B$ than marine sediments (Ishikawa and Nakamura, 1993). Similarly, marine sediments have higher $\delta^{18}O$ compared to continental sediments (see Bindeman et al., 2008 for a review). Simple Rayleigh distillation of marine sediment with an average initial composition of 5‰ suggest 85% B loss to reach a fluid end-member with an average composition of 0‰. Similarly, an average composition of -8‰ for continental sediments would lead to dehydration fluids with a composition of -14‰ after 90% B loss. Whereas sediments being subducted in the Aeolian arc are mostly continental (dust from Sahara and clastic sediments from river Nile; Klaver et al., 2015), sediments subducted in the Izu-Bonin arc, where

Sukumoyama is located, are mainly composed of marine sediments (ODP leg 1149; Plank et al., 2007) or clays (ODP leg 808; Plank and Langmuir, 1998), both of which have higher $\delta^{18}O$ than continental sediments. Oxygen, B and Cl isotopes all point toward two distinct sediment end-members that are coherent with the tectonic settings of Vulcano and Sukumoyama. Boron isotopic variability within each sediment end-member could represent variable degrees of dehydration or variable compositions of the subducted sediments. John et al. (2010) suggested that dehydrated subducted marine sediments could have $\delta^{37}Cl$ up to +4‰ (2‰ higher than highest measured values for fresh sediments, SM 1) due to Cl isotope fractionation during dehydration. Thus, a fluid derived from the dehydration of sediment with $\delta^{37}Cl$ as low as -5‰ would suggest a similar, but opposite as in fluid and not in solid, fractionation than suggested by John et al. (2010) (2.5‰ lower than lowest measured values for fresh sediments).

Combining B, O and Cl isotopes might thus allow better identification of different Cl reservoirs (serpentinites vs. AOC; marine vs continental sediments) involved in magma genesis beneath arcs. Whereas the serpentinite reservoir cannot be easily identified in the O and Cl isotopes system, it can be distinguished from AOC in the B and Cl isotopes system. Similarly, influence of marine vs. terrigenous sediments seems to be more easily tracked in B and Cl isotope systems.

5.1.4. Implications for the significance of $\delta^{37}Cl$ variability

Based on Figures 6 and 7, St. Vincent and Aoba mostly vary between AOC and serpentinite dehydration fluid end-members, suggesting a more pronounced influence from AOC and serpentinite fluids, compared to sediment fluids. Sediment fluids for St. Vincent can be marine and/or continental. The influence of three fluid end-members agrees with previous studies (Bouvier et al., 2008, 2010), and the suggested marine and continental sediments agrees with the sediment composition of the Barbados prism (Carpentier et al., 2008). Aoba

OHMIs also seem to reflect the mixed influence of AOC and serpentinite fluids, and a marine fluid sediment component. Vulcano and Sukumoyama OHMIs record the strongest sediment influence, with a possible influence from serpentinite fluids to explain the scatter. Iwate Volcano OHMIs follow the Cl-O isotopes trend (Figure 4) suggesting the influence of both AOC and sediment fluids, in agreement with Pb isotope measurements on Iwate Volcano OHMIs (Rose-Koga et al., 2014). This is confirmed in Figure 7, with $\delta^{11}B$ suggesting an influence from marine sediments.

Overall, these observations, based on the Cl-O-B isotope systematics, are consistent with the geological settings of the volcanoes that have been sampled and suggest that variability within a sample reflects multiple reservoirs adding Cl to the mantle wedge. Inter-arc variations in $\delta^{37}Cl$ most probably reflect global differences in the values for the main Cl reservoir (e.g., sediments vs. AOC and/or serpentinites).

5.2. Bulk rock vs. OHMI Cl isotope differences

New low $\delta^{37}Cl$ (< -1.5‰) are reported here, with Sukumoyama OHMIs having similar $\delta^{37}Cl$ compositions compared to Vulcano OHMIs. Interestingly, bulk rock values of samples from the same arcs exist and can be compared with OHMI data. Even if bulk rock data are not from the same sample, nor from the same volcanoes, as the OHMIs in this study, nearby volcanoes from the same arc should have similar source(s) of Cl input. For the Aeolian arc, bulk rock data exist for Etna and Stromboli, both having similar $\delta^{37}Cl$ (-0.96 to 0.69‰ for Stromboli and -0.7 to 0.1 for Etna; Liotta et al., 2017; Rizzo et al., 2013) despite their different magmatic histories (e.g., Tommasini et al., 2007). Also, as described in the introduction, Manzini et al. (2017) reported $\delta^{37}Cl$ in OHMIs from Stromboli, with values significantly different (-3.2 to -1.75‰) to Stromboli lavas, but similar to Vulcano OHMIs. We

480 thus conclude that bulk rock data from nearby volcanoes (e.g., Stromboli for Vulcano, and
481 Oshima and Niijima for Sukumoyama) could indeed be used to compare to OHMIs.

482 Bulk rock data are clearly different to our OHMI data, with a shift of up to 2‰ and 3.6‰
483 toward lower values for Vulcano and Sukumoyama OHMIs, respectively. As discussed in
484 section 5.1.1., this could not be induced by analytical bias. Rather, the combination of
485 negative $\delta^{37}Cl$ and $\delta^{11}B$ associated with elevated $\delta^{18}O$ suggest that the main source of Cl is
486 from a fluid issued from sediments, as discussed above.

487 Fortin et al. (2017) showed that Cl isotopes could be fractionated by up to 5‰ by Cl
488 diffusion during bubble growth, and potentially more in the case of diffusion not related to
489 bubble growth (depending on time scale). As mentioned by these authors, fractionation by Cl
490 diffusion during the formation of melt inclusions (i.e., via boundary layer entrapment) could
491 not generate lower isotopic compositions, but instead should generate higher $\delta^{37}Cl$ compared
492 to the initial composition. In section 5.1.1., the migration of Cl into a shrinkage bubble was
493 ruled out. If fractionation due to diffusion of Cl isotopes during shrinkage bubble growth
494 within the OHMIs does occur, it will cause ^{35}Cl to preferentially enter the bubble, leading to
495 $\delta^{37}Cl$ progressively increasing in the melt (Fortin et al., 2017). In this case, OHMIs should
496 have $\delta^{37}Cl$ compositions higher than bulk rock, whereas we have observed the opposite. As
497 no correlation has been observed between Cl or Cl/K_2O and $\delta^{37}Cl$ (Figure 5), the lower $\delta^{37}Cl$
498 values measured in Vulcano and Sumukoyama OHMIs compared to respective bulk rocks
499 probably do not represent degassing melts. On the contrary, bulk rocks have often suffered
500 some volatile degassing. For example, the Stromboli OHMIs measured for $\delta^{37}Cl$ have Cl
501 contents from 0.14 to 0.46 wt% (Manzini et al., 2017), whereas bulk rocks only contain 0.03
502 to 0.08 wt% (Liotta et al., 2017). Assuming fractionation due to diffusion of Cl isotopes
503 during bubble growth in the magma (as opposed to shrinkage bubble growth in OHMIs),
504 gases enriched in ^{35}Cl could be created. This will thus create low $\delta^{37}Cl$ gases and a magma

505 with $\delta^{37}Cl$ increasing with the increase of degassing. Interestingly, low $\delta^{37}Cl$ has been
506 measured in Hakone (northern part of Izu-Bonin arc, down to -5.41‰; Barnes et al., 2008)
507 and Stromboli gases (down to -2.2‰; Liotta et al., 2017). OHMIs from Sukumoyama and
508 Vulcano could thus represent relatively primary undegassed melt, whereas the bulk rocks
509 record Cl loss during degassing, enriching the melt in ^{37}Cl due to diffusive fractionation
510 during bubble growth. In that case, the bulk rocks lose the original $\delta^{37}Cl$ signature of the
511 source of the Cl input.

512 **6. Conclusions**

513 This study expands the dataset of Cl isotopes in OHMIs from arc settings and is the first
514 coupling $\delta^{37}Cl$ with two other isotopic systems in OHMIs. This dataset suggests that Cl
515 isotopes variation in OHMIs within a single sample most probably record Cl input from
516 different Cl reservoirs, rather than heterogeneity from a single reservoir. Inter-arc variability
517 in $\delta^{37}Cl$ might reflect differences in the main Cl reservoirs (e.g., larger influences of
518 sediments in some arcs).

519 Indirect comparison of OHMI data from Vulcano and Sukumoyama and bulk rock data
520 from the same arc reveal large (2 to 4‰) differences, with OHMIs having lower $\delta^{37}Cl$ than
521 bulk rocks. This difference most probably reflects diffusive fractionation of Cl isotopes during
522 degassing of the lavas. OHMIs have relatively primary compositions whereas the bulk lavas
523 have lost the original $\delta^{37}Cl$ signature during degassing. This conclusion is supported by some
524 low (<0‰) $\delta^{37}Cl$ gases measured at volcanoes in both arcs.

525 Chlorine isotope measurements by SIMS in MIs could thus provide valuable and unique
526 access to relatively primary (undegassed) $\delta^{37}Cl$ compositions. Better constraints on the source
527 of Cl is important to better understand the behavior or Cl in different contexts and ultimately,
528 refine the Cl budget.

Acknowledgments

Research was supported by the KIP-6 PCI grant CASA to LPB. EFR-K acknowledges the French Government Laboratory of Excellence initiative n°ANR-10- LABEX-0006. The authors would like to thank Nicole Métrich for thoughtful comments, Janne Koornneef, two anonymous reviewers and the editor, Frederic Moynier, for the helpful reviews and suggestions.

References

Aiuppa, A., Baker, D.R., Webster, J.D., 2009. Halogens in volcanic systems. Chem. Geol. 263, 1–18. https://doi.org/10.1016/j.chemgeo.2008.10.005

Alt, J.C., 2003. Stable isotopic composition of upper oceanic crust formed at a fast spreading ridge, ODP Site 801. Geochemistry, Geophys. Geosystems 4, 1–11. https://doi.org/10.1029/2002GC000400

Alt, J.C., Bach, W., 2006. Oxygen isotope composition of a section of lower oceanic crust, ODP Hole 735B. Geochemistry, Geophys. Geosystems 7. https://doi.org/10.1029/2006GC001385

Barnes, J.D., Beltrando, M., Lee, C.T.A., Cisneros, M., Loewy, S., Chin, E., 2014. Geochemistry of Alpine serpentinites from rifting to subduction: A view across paleogeographic domains and metamorphic grade. Chem. Geol. 389, 29–47. https://doi.org/10.1016/j.chemgeo.2014.09.012

Barnes, J.D., Cisneros, M., 2012. Mineralogical control on the chlorine isotope composition of altered oceanic crust. Chem. Geol. 326–327, 51–60. https://doi.org/10.1016/j.chemgeo.2012.07.022

Barnes, J.D., Selverstone, J., Sharp, Z.D., 2006. Chlorine isotope chemistry of serpentinites from Elba, Italy, as an indicator of fluid source and subsequent tectonic history. Geochemistry, Geophys. Geosystems 7. https://doi.org/10.1029/2006GC001296

553 Barnes, J.D., Sharp, Z.D., Fischer, T.P., 2008. Chlorine isotope variations across the Izu-Bonin-
554 Mariana arc. Geology 36, 883. https://doi.org/10.1130/G25182A.1

555 Barnes, J.D., Sharp, Z.D., Fischer, T.P., Hilton, D.R., Carr, M.J., 2009. Chlorine isotope variations
556 along the Central American volcanic front and back arc. Geochemistry, Geophys. Geosystems 10,
557 n/a-n/a. https://doi.org/10.1029/2009GC002587

558 Barnes, J.D., Straub, S.M., 2010. Chorine stable isotope variations in Izu Bonin tephra: Implications
559 for serpentinite subduction. Chem. Geol. 272, 62–74.
560 https://doi.org/10.1016/j.chemgeo.2010.02.005

561 Bindeman, I., 2008. Oxygen Isotopes in Mantle and Crustal Magmas as Revealed by Single Crystal
562 Analysis. Rev. Mineral. Geochemistry 69, 445–478. https://doi.org/10.2138/rmg.2008.69.12

563 Bonifacie, M., Busigny, V., Mével, C., Philippot, P., Agrinier, P., Jendrzejewski, N., Scambelluri, M.,
564 Javoy, M., 2008. Chlorine isotopic composition in seafloor serpentinites and high-pressure
565 metaperidotites. Insights into oceanic serpentinization and subduction processes. Geochim.
566 Cosmochim. Acta 72, 126–139. https://doi.org/10.1016/j.gca.2007.10.010

567 Boschi, C., Bonatti, E., Ligi, M., Brunelli, D., Cipriani, A., Dallai, L., D'Orazio, M., Früh-Green,
568 G.L., Tonarini, S., Barnes, J.D., Bedini, R.M., 2013. Serpentinization of mantle peridotites along an
569 uplifted lithospheric section, mid atlantic ridge at 11° N. Lithos 178, 3–23.
570 https://doi.org/10.1016/j.lithos.2013.06.003

571 Bouvier, A.-S., Metrich, N., Deloule, E., 2008. Slab-Derived Fluids in the Magma Sources of St.
572 Vincent (Lesser Antilles Arc): Volatile and Light Element Imprints. J. Petrol. 49, 1427–1448.
573 https://doi.org/10.1093/petrology/egn031

574 Bouvier, A.-S., Deloule, E., Metrich, N., 2010. Fluid Inputs to Magma Sources of St. Vincent and
575 Grenada (Lesser Antilles): New Insights from Trace Elements in Olivine-hosted Melt Inclusions. J.
576 Petrol. 51, 1597–1615. https://doi.org/10.1093/petrology/egq031

577 Bucholz, C.E., Gaetani, G. a., Behn, M.D., Shimizu, N., 2013. Post-entrapment modification of
578 volatiles and oxygen fugacity in olivine-hosted melt inclusions. Earth Planet. Sci. Lett. 374, 145–

155. https://doi.org/10.1016/j.epsl.2013.05.033

Carpentier, M., Chauvel, C., Mattielli, N., 2008. Pb–Nd isotopic constraints on sedimentary input into the Lesser Antilles arc system. Earth Planet. Sci. Lett. 272, 199–211. https://doi.org/10.1016/j.epsl.2008.04.036

Chaussidon, M., Jambon, A., 1994. Boron content and isotopic composition of oceanic basalts: Geochemical and cosmochemical implications. Earth Planet. Sci. Lett. 121, 277–291.

Fortin, M.-A., Watson, E.B., Stern, R., 2017. The isotope mass effect on chlorine diffusion in dacite melt, with implications for fractionation during bubble growth. Earth Planet. Sci. Lett. 480, 15–24. https://doi.org/https://doi.org/10.1016/j.epsl.2017.09.042

Ishikawa, T., Nakamura, E., 1993. Boron isotope systematics of marine sediments. Earth Planet. Sci. Lett. 117, 567–580. https://doi.org/10.1016/0012-821X(93)90103-G

John, T., Scambelluri, M., Frische, M., Barnes, J.D., Bach, W., 2011. Dehydration of subducting serpentinite: Implications for halogen mobility in subduction zones and the deep halogen cycle. Earth Planet. Sci. Lett. 308, 65–76. https://doi.org/10.1016/j.epsl.2011.05.038

John, T., Scherer, E.E., Schenk, V., Herms, P., Halama, R., Garbe-Schönberg, D., 2010. Subducted seamounts in an eclogite-facies ophiolite sequence: the Andean Raspas Complex, SW Ecuador. Contrib. to Mineral. Petrol. 159, 265–284. https://doi.org/10.1007/s00410-009-0427-0

Klaver, M., Djuly, T., de Graaf, S., Sakes, A., Wijbrans, J., Davies, G., Vroon, P., 2015. Temporal and spatial variations in provenance of Eastern Mediterranean Sea sediments: Implications for Aegean and Aeolian arc volcanism. Geochim. Cosmochim. Acta 153, 149–168. https://doi.org/10.1016/j.gca.2015.01.007

Liebscher, A., Barnes, J.D., Sharp, Z., 2006. Chlorine isotope vapor–liquid fractionation during experimental fluid-phase separation at 400 °C/23 MPa to 450 °C/42 MPa. Chem. Geol. 234, 340–345. https://doi.org/10.1016/j.chemgeo.2006.04.009

Liotta, M., Rizzo, A.L., Barnes, J.D., D'Auria, L., Martelli, M., Bobrowski, N., Wittmer, J., 2017. Chlorine isotope composition of volcanic rocks and gases at Stromboli volcano (Aeolian Islands,

Italy): Inferences on magmatic degassing prior to 2014 eruption. J. Volcanol. Geotherm. Res. 336, 168–178. https://doi.org/https://doi.org/10.1016/j.jvolgeores.2017.02.018

Manzini, M., Bouvier, A.-S., Barnes, J.D., Bonifacie, M., Rose-Koga, E.F., Ulmer, P., Métrich, N., Bardoux, G., Williams, J., Layne, G.D., Straub, S., Baumgartner, L.P., John, T., 2017. SIMS chlorine isotope analyses in melt inclusions from arc settings. Chem. Geol. 449. https://doi.org/10.1016/j.chemgeo.2016.12.002

Mather, T. a., Witt, M.L.I., Pyle, D.M., Quayle, B.M., Aiuppa, a., Bagnato, E., Martin, R.S., Sims, K.W.W., Edmonds, M., Sutton, a. J., Ilyinskaya, E., 2012. Halogens and trace metal emissions from the ongoing 2008 summit eruption of Kīlauea volcano, Hawai`i. Geochim. Cosmochim. Acta 83, 292–323. https://doi.org/10.1016/j.gca.2011.11.029

Métrich, N., Deloule, E., 2014. Water content, δD and δ11B tracking in the Vanuatu arc magmas (Aoba Island): Insights from olivine-hosted melt inclusions. Lithos 206–207, 400–408. https://doi.org/10.1016/j.lithos.2014.08.011

Moore, L.R., Gazel, E., Tuohy, R., Lloyd, A.S., Esposito, R., Steele-MacInnis, M., Hauri, E.H., Wallace, P.J., Plank, T., Bodnar, R.J., 2015. Bubbles matter: An assessment of the contribution of vapor bubbles to melt inclusion volatile budgets. Am. Mineral. 100, 806–823.

Muehlenbachs, K., 1986. Alteration of the oceanic crust and the 18 O history of seawater. Rev. Mineral. Geochemistry 16, 425–444.

Nichols, A.R.L., Wysoczanski, R.J., Tani, K., Tamura, Y., Baker, J.A., Tatsumi, Y., 2012. Melt inclusions reveal geochemical cross-arc variations and diversity within magma chambers feeding the Higashi-Izu Monogenetic Volcano Field, Izu Peninsula, Japan. Geochemistry, Geophys. Geosystems 13, 1–28. https://doi.org/10.1029/2012GC004222Peacock, S.M., Hervig, R.L., 1999. Boron isotopic composition of subduction-zone metamorphic rocks. Chem. Geol. 160, 281–290.

Peccerillo, A., De Astis, G., Faraone, D., Forni, F., Frezzotti, M.L., 2013. Chapter 15 Compositional variations of magmas in the Aeolian arc: implications for petrogenesis and geodynamics. Geol. Soc. London, Mem. 37, 491–510. https://doi.org/10.1144/M37.15

631 Plank, T., Kelley, K.A., Murray, R.W., Stern, L.Q., 2007. Chemical composition of sediments
632 subducting at the Izu-Bonin trench. Geochemistry, Geophys. Geosystems 8, 1–16.
633 https://doi.org/10.1029/2006GC001444

634 Plank, T., Langmuir, C.H., 1998. The chemical composition of subducting sediment and its
635 consequences for the crust and mantle. Chem. Geol. 145, 325–394.

636 Rizzo, A.L., Caracausi, A., Liotta, M., Paonita, A., Barnes, J.D., Corsaro, R. a., Martelli, M., 2013.
637 Chlorine isotope composition of volcanic gases and rocks at Mount Etna (Italy) and inferences on
638 the local mantle source. Earth Planet. Sci. Lett. 371–372, 134–142.
639 https://doi.org/10.1016/j.epsl.2013.04.004

640 Rose, E.F., Shimizu, N., Layne, G.D., Grove, T.L., 2001. Melt production beneath Mt. Shasta from
641 boron data in primitive melt inclusions. Science 293, 281–3.
642 https://doi.org/10.1126/science.1059663

643 Rose-Koga, E.F., Koga, K.T., Hamada, M., Hélouis, T., Whitehouse, M.J., Shimizu, N., 2014. Volatile
644 (F and Cl) concentrations in Iwate olivine-hosted melt inclusions indicating low-temperature
645 subduction. Earth, Planets Sp. 66, 81. https://doi.org/10.1186/1880-5981-66-81

646 Rosner, M., Wiedenbeck, M., Ludwig, T., 2008. Composition-Induced Variations in SIMS
647 Instrumental Mass Fractionation during Boron Isotope Ratio Measurements of Silicate Glasses.
648 Geostand. Geoanalytical Res. 32, 27–38. https://doi.org/10.1111/j.1751-908X.2008.00875.x

649 Schauble, E.A., Rossman, G.R., Taylor, H.P., J., 2003. Theoretical estimates of equilibrium chlorine-
650 isotope fractionations. Geochim. Cosmochim. Acta 67, 3267–3281. https://doi.org/10.1016/S0016-
651 7037(00)01375-3

652 Sharp, Z.D., Barnes, J.D., Brearley, a J., Chaussidon, M., Fischer, T.P., Kamenetsky, V.S., 2007.
653 Chlorine isotope homogeneity of the mantle, crust and carbonaceous chondrites. Nature 446, 1062–
654 1065. https://doi.org/10.1038/nature05748

655 Smith, H.J., Leeman, W.P., Davidson, J., Spivack, A.J., 1997. The B isotopic composition of arc lavas
656 from Martinique, Lesser Antilles. Earth Planet. Sci. Lett. 146, 303–314.

https://doi.org/10.1016/S0012-821X(96)00209-9

Smith, H.J., Spivack, A.J., Staudigel, H., Hart, S.R., 1995. The boron isotopic composition of altered oceanic crust. Chem. Geol. 126, 119–135.

Sorbadere, F., Schiano, P., Métrich, N., Garaebiti, E., 2011. Insights into the origin of primitive silica-undersaturated arc magmas of Aoba volcano (Vanuatu arc). Contrib. to Mineral. Petrol. 162, 995–1009. https://doi.org/10.1007/s00410-011-0636-1

Tenthorey, E., Hermann, J., 2004. Composition of fluids during serpentinite breakdown in subduction zones: Evidence for limited boron mobility. Geology 32, 865–868.

Tommasini, S., Heumann, A., Avanzinelli, R., Francalanci, L., 2007. The Fate of High-Angle Dipping Slabs in the Subduction Factory: an Integrated Trace Element and Radiogenic Isotope (U, Th, Sr, Nd, Pb) Study of Stromboli Volcano, Aeolian Arc, Italy. J. Petrol. 48, 2407–2430.

Trommsdorff, V., Sánchez-Vizcaíno, V.L., Gómez-Pugnaire, M.T., Müntener, O., 1998. High pressure breakdown of antigorite to spinifex-textured olivine and orthopyroxene, SE Spain. Contrib. to Mineral. Petrol. 132, 139–148. https://doi.org/10.1007/s004100050412

Urann, B.M., Le Roux, V., Hammond, K., Marschall, H.R., Lee, C.-T.A., Monteleone, B.D., 2017. Fluorine and chlorine in mantle minerals and the halogen budget of the Earth's mantle. Contrib. to Mineral. Petrol. 172, 51. https://doi.org/10.1007/s00410-017-1368-7

Vils, F., Tonarini, S., Kalt, A., Seitz, H.-M., 2009. Boron, lithium and strontium isotopes as tracers of seawater–serpentinite interaction at Mid-Atlantic ridge, ODP Leg 209. Earth Planet. Sci. Lett. 286, 414–425. https://doi.org/10.1016/j.epsl.2009.07.005

You, C., Spivack, A.J., Gieskes, J.M., Martin, J.B., Davisson, M.L., 1996. Boron contents and isotopic compositions in pore waters : a new approach to determine temperature induced artifacts-geochemical implications 129, 351–361.

Zheng, Y.F., 1993. Calculation of oxygen isotope fractionation in hydroxyl-bearing silicates. Earth Planet. Sci. Lett. 120, 247–263. https://doi.org/10.1016/0012-821X(93)90243-3

Zheng, Y.-F., Satir, M., Metz, P., Sharp, Z.D., 1999. Oxygen isotope exchange processes and

683 disequilibrium between calcite and forsterite in an experimental C-O-H fluid. Geochim.
684 Cosmochim. Acta 63, 1781–1786.

685

Captions:

Figure 1: Compilation of published $\delta^{37}Cl$ for terrestrial bulk rocks and olivine-hosted melt inclusions (OHMIs). Sukumoyama and Iwate Volcano OHMIs are new data, the remaining are published data. A summary of the database can be found in SM 1, with all the associated references. OHMIs are plotted using symbols, whereas bulk rocks are represented with bars. Sediments and serpentinite bulk rocks are plotted with dark colors representing fresh rocks, and light colors metamorphic rocks.

Figure 2: SiO_2 compared to total alkalis ($Na_2O + K_2O$) (TAS diagram) for OHMIs of St. Vincent (squares), Aeolian islands (triangles), Aoba (diamonds), Sukumoyama (yellow circles) and Iwate (brown circles). The OHMIs have basanitic to basaltic compositions.

Figure 3: SiO_2 compared to Cl content in the studied OHMIs. Symbols as in Figure 2. No variation of Cl content with increasing SiO_2 is observed, suggesting Cl is not degassing during OHMIs entrapment.

Figure 4: Chlorine isotopes compared to SiO_2 (A) and $Na_2O + K_2O$ (B) in the OHMIs. No correlation between $\delta^{37}Cl$ and the major elements are seen, proving that the matrix effect has been corrected. Also, the absence of any correlation suggests that Cl isotopes are not affected by extent of magmatic evolution.

Figure 5: Chlorine isotopes compared to Cl/K_2O ratios. The absence of correlation between $\delta^{37}Cl$ and Cl/K_2O supports the absence of Cl degassing at the time of entrapment. Thus, the variation of $\delta^{37}Cl$ in the OHMIs cannot be linked to degassing.

Figure 6: O isotopes compared to Cl isotopes in St. Vincent (squares), Aeolian islands (triangles), Aoba (diamonds), Sukumoyama (yellow circles) and Iwate (brown circles) OHMIs. All OHMIs define a negative relationship between $\delta^{37}Cl$ and $\delta^{18}O$. Sukumoyama and Aeolian OHMIs record the strongest influence from sediment fluids, whereas St. Vincent and Iwate Volcano record fluids derived from the dehydration of both AOC and sediments. Aoba also reflect influences from sediment fluids, and either AOC or serpentinite fluids. Fields for sediments, AOC and serpentinites are based on bulk rock data. Bulk rock O and Cl isotope data were obtained on the same samples only for oceanic serpentinites. Cl isotope data are from the same references as in Figure 1 and SM 1. Oxygen isotope data for AOC are from Alt (2003) and Alt & Bach (2006). Only fresh oceanic serpentinites have been reported here (data for $\delta^{18}O$ are from Bonifacie et al. (2008) and Boschi et al. (2013)). Fresh sedimentary rock $\delta^{18}O$ data are from the compilation of Bindeman (2008).

Figure 7: B isotopes compared to Cl isotopes. Symbols are as in Figure 5. For comparison, different reservoirs have been plotted (see text for references). As for Figure 4, only fresh sediments and serpentinites have been reported. Reservoirs defined by dashed lines are a compilation of data in which none of the samples have combined $\delta^{11}B$ and $\delta^{37}Cl$ measurements. OHMIs suggest the influence of four different fluid end-members, one each for AOC and serpentinites, and two distinct end-members for sediments, one for marine and one for continental sediments.

Table 1: B, O and Cl isotopes in OHMIs

Supplementary material

SM1: Database for Cl isotopes in terrestrial bulk rocks and OHMIs

SM2: SIMS calibrations

SM3: Summary of major element and stable isotopes of OHMIs used in Manzini et al. (2017)

SM4: Summary of major elements and stable isotopes of OHMIs from Iwate Volcano and Sukumoyama

SM5: Comparison of major element compositions of OHMIs and whole rocks.

Figure 1

Click here to download high resolution image

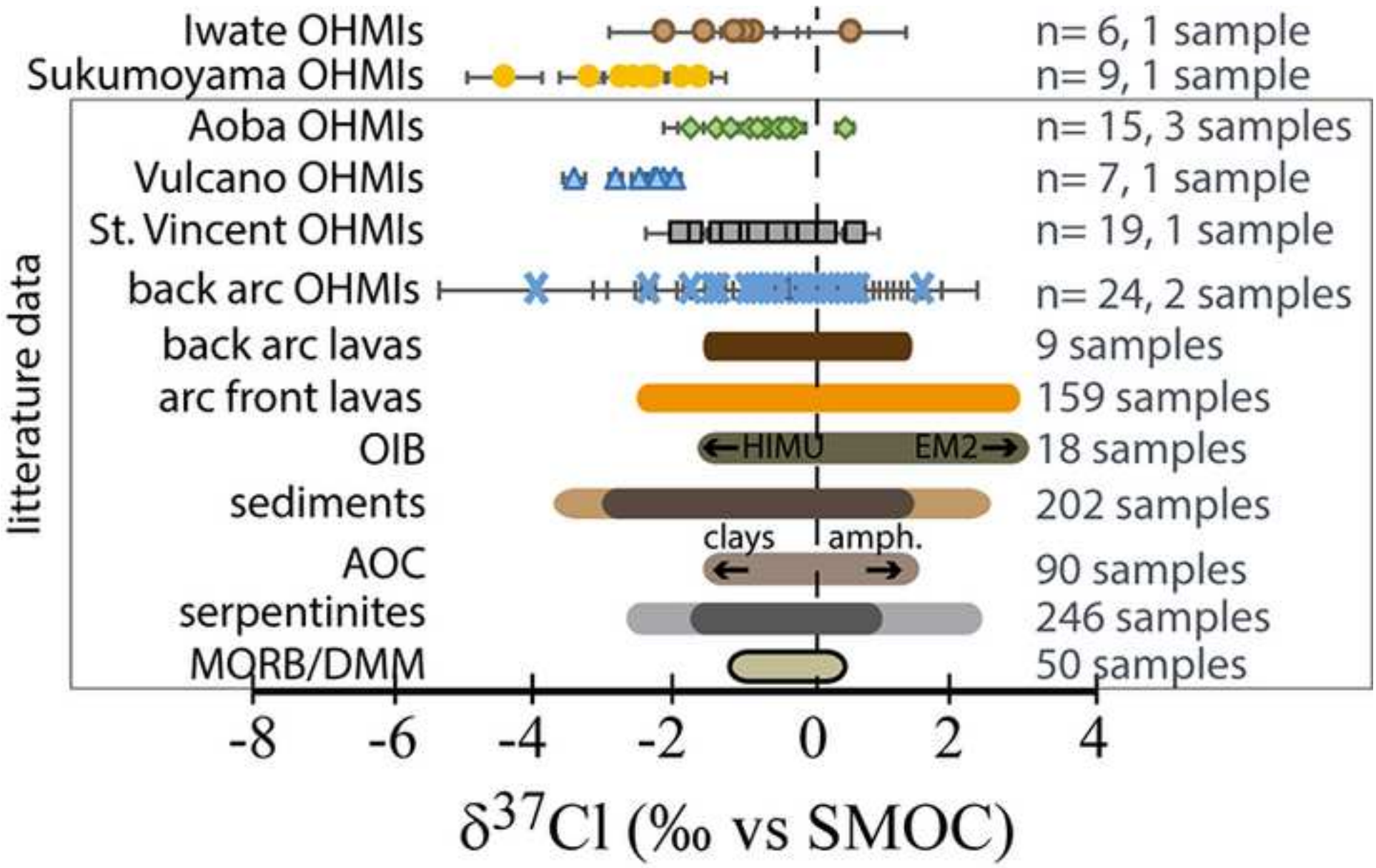

Figure 2

Click here to download high resolution image

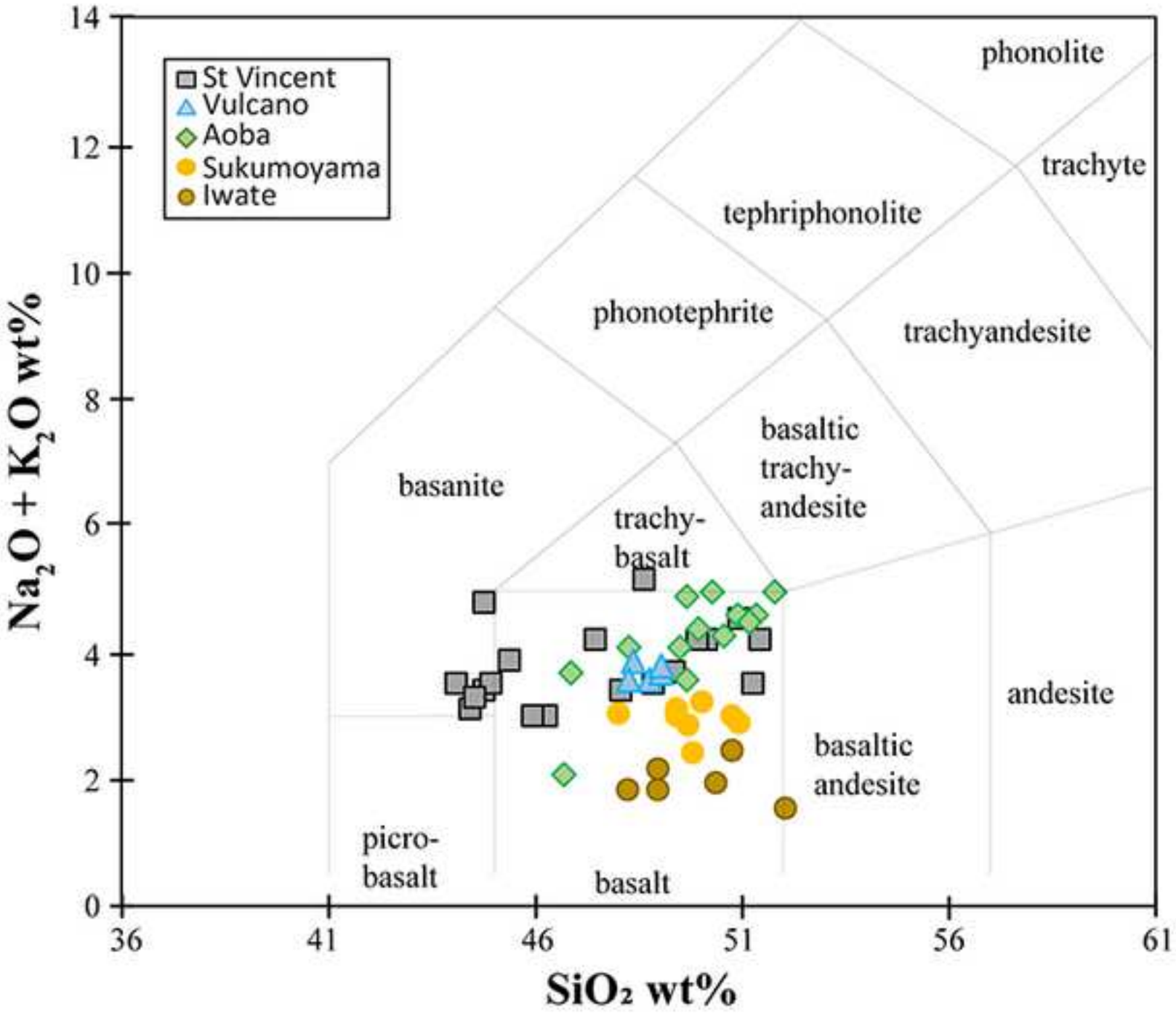

Figure 3

Click here to download high resolution image

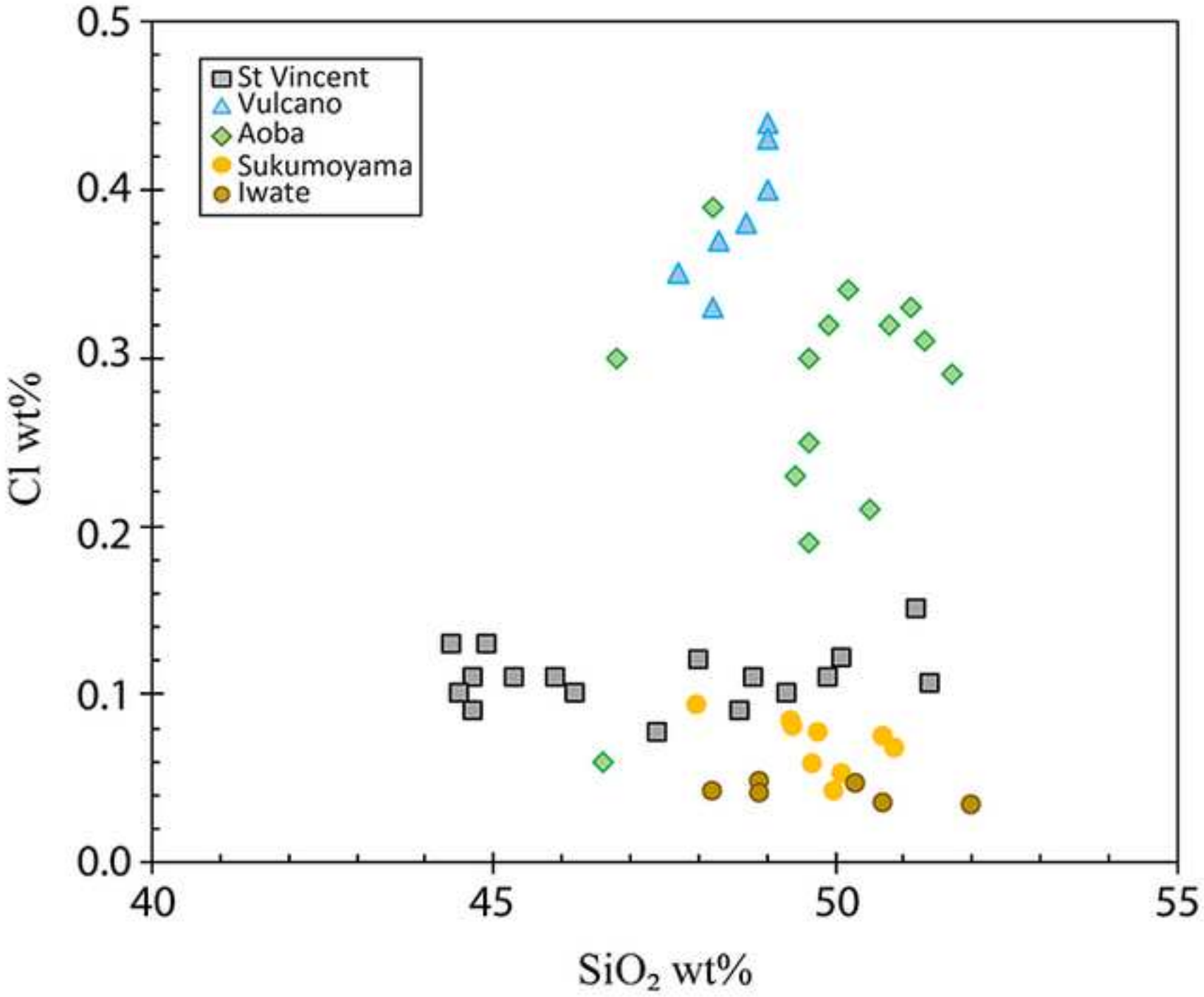

Figure 4

Click here to download high resolution image

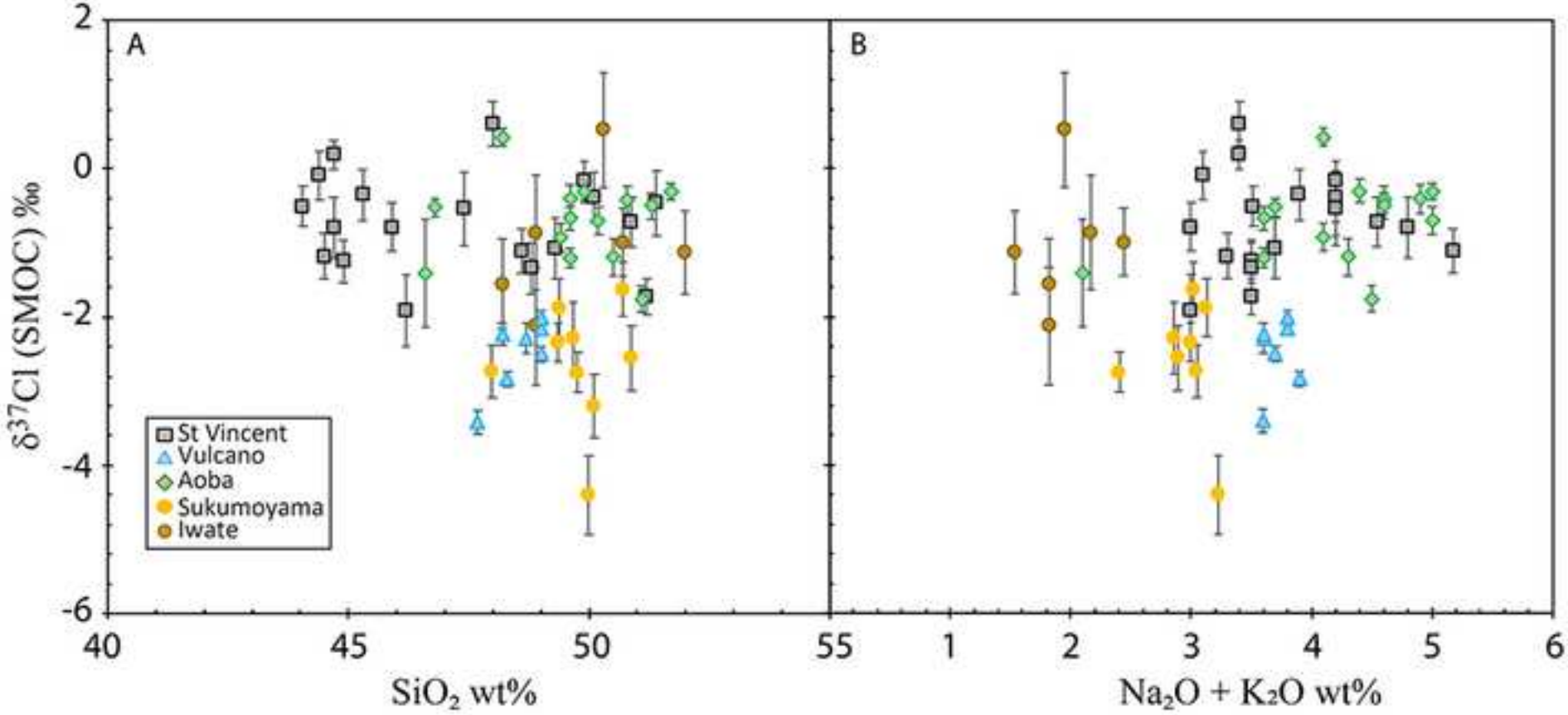

Figure 5

Click here to download high resolution image

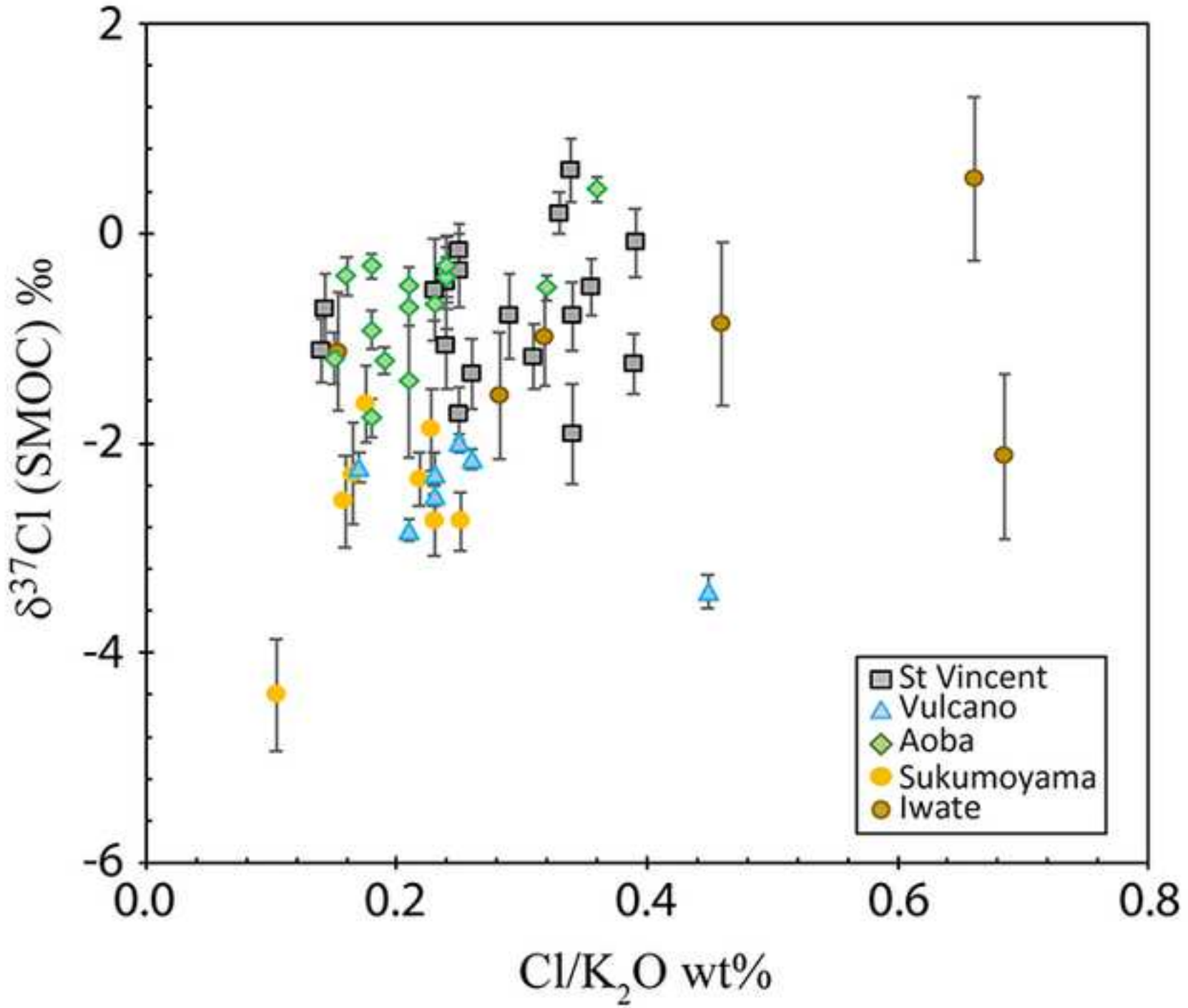

Figure 6

Click here to download high resolution image

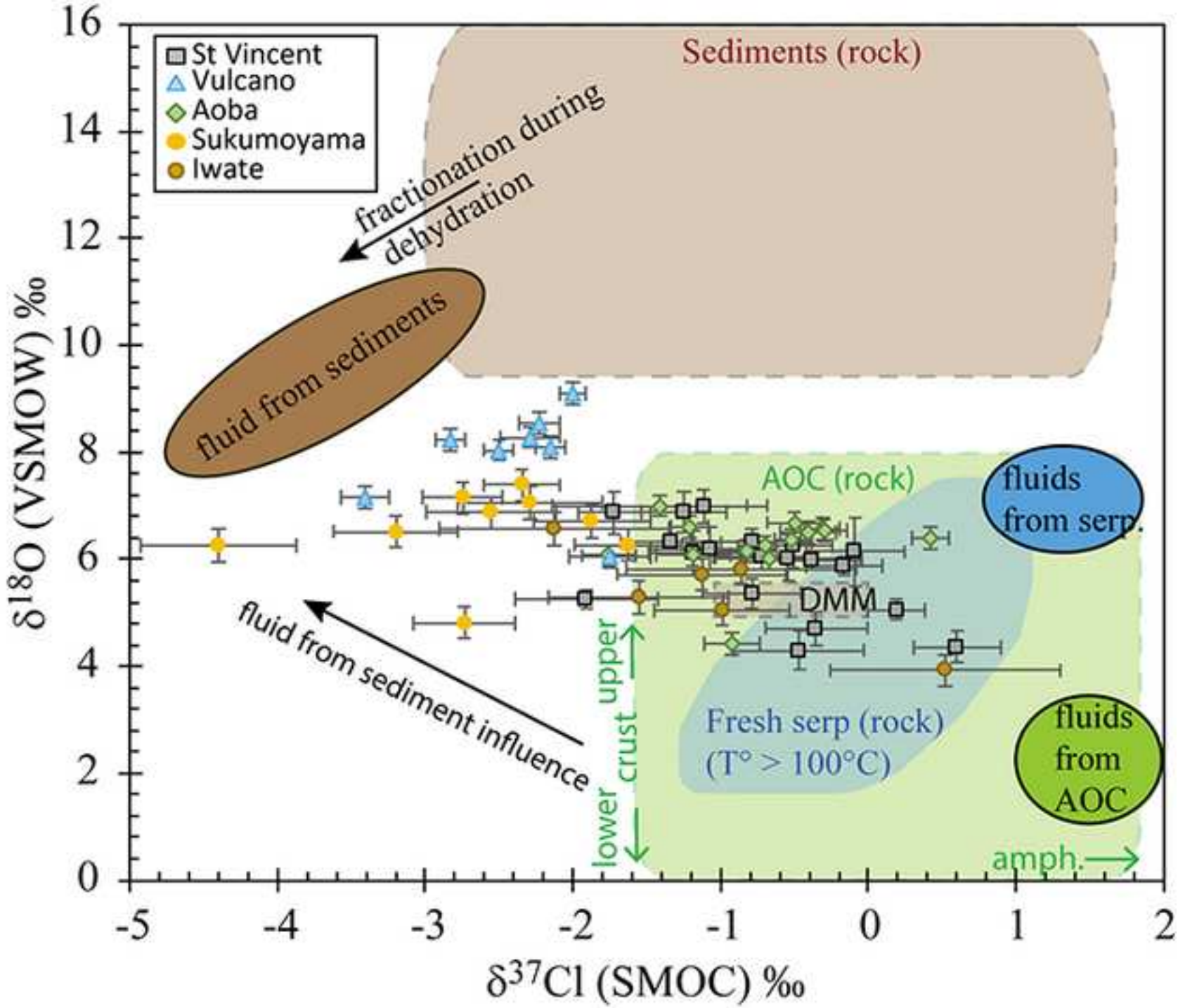

Figure 7

Click here to download high resolution image

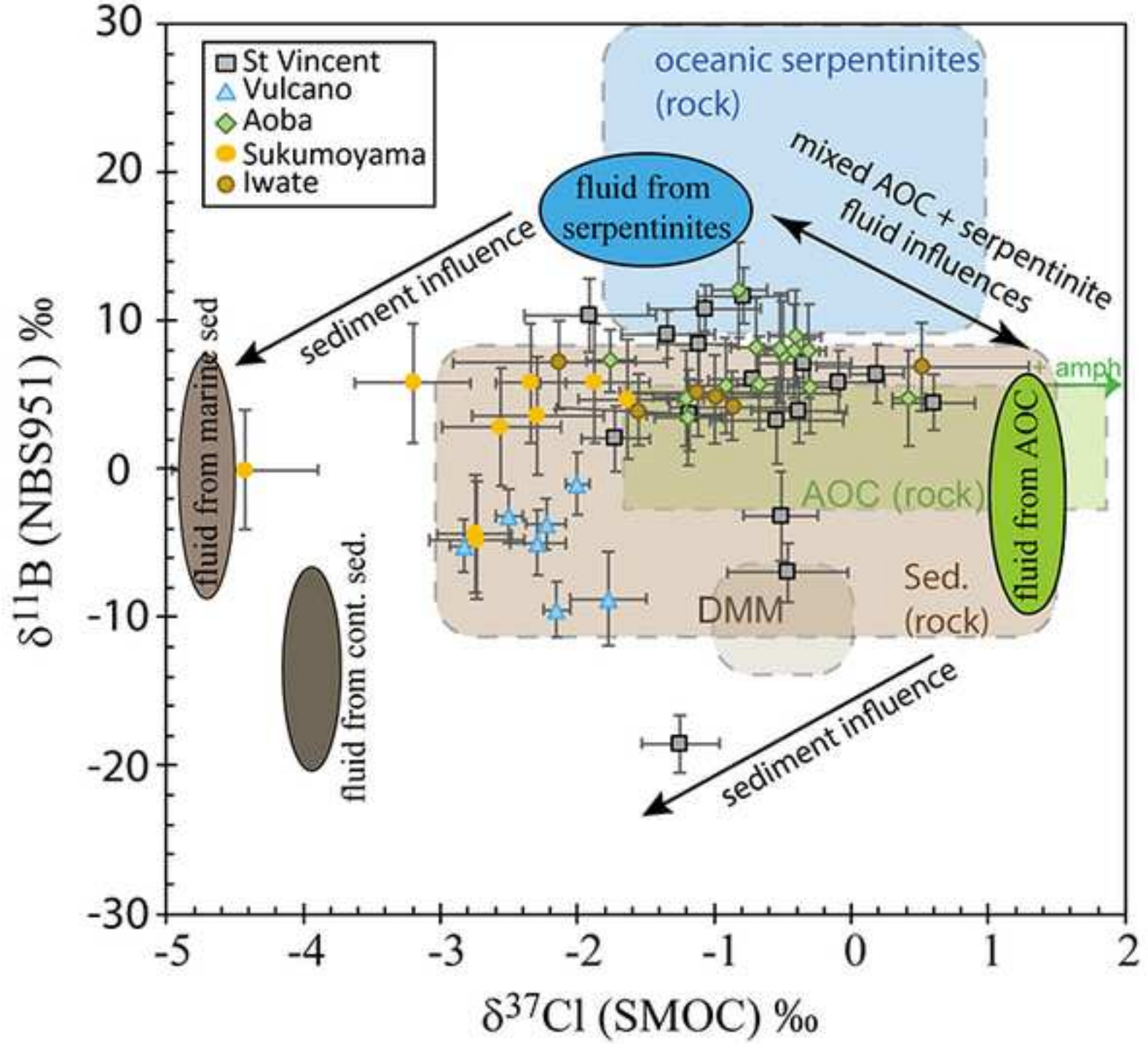

Figure (high-resolution) 1

Click here to download Figure (high-resolution): Fig1.tif

Figure (high-resolution) 2

Click here to download Figure (high-resolution): Fig2_TAS.tif

Figure (high-resolution) 3

Click here to download Figure (high-resolution): Fig3_Cl-vs-SiO2.tif

Figure (high-resolution) 4

Click here to download Figure (high-resolution): Fig4_d37Cl-vs-SiO2&-vs-alcalins.tif

Figure (high-resolution) 5

Click here to download Figure (high-resolution): Fig5_d37Cl-vs-Cl-K2O.tif

Figure (high-resolution) 6

Click here to download Figure (high-resolution): Fig6_new.tif

Figure (high-resolution) 7

Click here to download Figure (high-resolution): Fig7_new.tif

Table1
Click here to download Table: table1.xlsx

Table 1: B, O and Cl isotopes in OHMIs

	$\delta^{37}Cl$	2σ	$\delta^{18}O$	2σ	$\delta^{11}B$	2σ
OHMIs from St. Vincent (Lesser Antilles arc),						
svn4b-24	*-0.5*	0.4	4.3	0.4	-7.0	2.0
svn4b-36	*-0.4*	0.3	6.0	0.2	3.9	2.2
svn4b-60	*-0.5*	0.5	6.0	0.4	3.2	2.9
svn4b-90a	*-0.2*	0.3	5.9	0.2	n.d.	n.d.
svn4b-90b	*-1.1*	0.3	7.0	0.3	8.4	2.5
svn4b-90v	*-0.7*	0.3	6.1	0.3	6.0	n.d.
svn4b-164a	*0.2*	0.2	5.1	0.2	6.4	2.0
svn4b-171a	*-1.2*	0.3	6.9	0.4	-18.5	1.9
svn4b-176a	*-0.4*	0.3	4.7	0.3	7.1	2.0
svn4b-181a	*0.6*	0.3	4.4	0.3	4.5	1.9
svn4b-181b	*-1.7*	0.2	6.9	0.4	2.0	2.2
svn4b-184	*-0.5*	0.3	6.3	0.4	-3.2	3.0
svn4b-186	*-0.8*	0.4	6.3	0.3	n.d.	n.d.
svn4b-MM1a	*-1.3*	0.3	6.3	0.1	9.1	1.6
svn4b-MM2	*-1.1*	0.4	6.2	0.4	10.8	1.6
svn4b-MM3a	*-0.1*	0.3	6.1	0.7	5.9	2.0
svn4b-MM7	*-1.9*	0.5	5.3	0.2	10.3	2.4
svn4b-MM15a	*-1.2*	0.3	6.1	0.4	3.7	2.4
svn4b-MM22	*-0.8*	0.3	5.4	0.3	11.7	1.9
OHMIs from Aoba (Vanuatu arc)						
17–10-b	*-0.4*	0.2	n.d.	n.d.	7.9	3.2
17–10-c	*-0.3*	0.1	6.6	0.2	7.9	3.2
17–16-a	*-1.2*	0.1	6.6	0.2	4.8	3.2
17–16-b	*-0.7*	0.2	6.0	0.2	5.8	3.2
3–9	*-1.4*	0.7	7.0	0.2	n.d.	n.d.
3–10 h3–1-a	*-0.9*	0.2	4.4	0.2	5.6	3.2
3–1-a	*-0.5*	0.2	6.7	0.2	7.7	3.6
3–1-b	*-0.7*	0.2	6.3	0.2	8.2	3.3
3-h1-a	*-0.5*	0.1	6.4	0.2	8.1	3.7
3-4	*-0.82*	0.2	6.2	0.2	12.0	3.2
3–5	*0.4*	0.1	6.4	0.2	4.7	3.2
3–6	*-1.8*	0.2	6.1	0.2	7.3	2.1
15–1-a	*-0.3*	0.2	6.5	0.2	5.5	3.2
15–10-a	*-1.2*	0.3	6.1	0.2	3.4	3.2
15–10-b	*-0.4*	0.2	6.5	0.2	8.9	3.2
OHMIs from Vulcano (Aeolian arc)						
S1	*-2.3*	0.2	8.3	0.2	-4.9	2.2
S2	*-2.8*	0.1	8.2	0.2	-5.1	1.8
S3	*-2.5*	0.1	8.0	0.2	-3.1	1.8
S7-a	*-2.2*	0.1	8.1	0.2	-9.5	1.9
S7-b	*-2.0*	0.1	9.1	0.2	-1.0	2.1
S9	*-2.2*	0.1	8.5	0.2	-3.7	1.7

SM1 - database

Click here to download Supplementary material for online publication only: SM1.xlsx

SM2 - calibrations

Click here to download Supplementary material for online publication only: Supplementary Material 2_final.docx

SM3

Click here to download Supplementary material for online publication only: SM3.xlsx

SM4

Click here to download Supplementary material for online publication only: SM4.xlsx

SM5

Click here to download Supplementary material for online publication only: Supplementary material 5_final.docx